Int J Fract (2013) 179:1–7
DOI 10.1007/s10704-012-9752-9

ORIGINAL PAPER

Orthogonal meshless finite volume method applied to elastodynamic crack problems

M. R. Moosavi

Received: 29 August 2011 / Accepted: 1 November 2011 / Published online: 25 July 2012

Abstract An orthogonal meshless finite volume method has been presented to solve some elastodynamic crack problems. An orthogonal weighted basis function is used to construct shape function so there is no problem of singularity in this new form. In this work, for three-dimensional dynamic fracture problems, a new displacement function is used at the tip of the crack to give a new OMFVM. When the new OMFVM is used, the singularity of the stresses at the tip of the crack can be shown to be better than that in the primal OMFVM. High computational efficiency and precision are other benefits of the method. Solving some sample crack problems of thin-walled structures show a good performance of this method.

Keywords Meshless method · Finite volume method · Orthogonal moving least square · Elastodynamics · Crack

1 Introduction

The modeling of dynamic fracture or failure problems remains one of the most challenging problems in mechanics. Dynamic failure modeling is an essential ingredient in the lifetime prediction of critical components in structures such as aircraft, automobiles and pressure vessels. It also plays an important role in the development of advanced materials such as composites and in understanding their durability and integrity. Finite element methods (FEMs) based on singular elements as well as enriched elements are reasonably effective in the analysis of stationary cracks. However, the modeling of growing cracks presents automatic mesh generation difficulties and, in certain cases, manual intervention is required. No general purpose computational method currently exists which can handle crack growth in complex 3D bodies for arbitrary constitutive response without recourse to extensive remeshing.

Since the inception of smoothed particle hydrodynamics (Monaghan 1982, 1988), a wide variety of meshless (or meshfree) methods have been proposed, as outlined in recent surveys. They are believed to be better suited to solve problems with moving boundaries, such as the modeling of crack propagation. The most widely used meshless method at present, the element-free Galerkin method (EFGM) (Belytschko et al. 1994), is developed for crack modelling in a number of references. The extended finite element method (XFEM) is probably the premier numerical technique for crack modelling and requires minimal or even no remeshing as cracks grow. Much of the well-developed convergence and error estimation theory developed for the FEM can be applied to the XFEM, which is not the case at present for most meshless methods. However, stresses from the XFEM are not smooth, unlike those from the EFGM, and any meshing overhead may preclude the efficient use of very large

M. R. Moosavi (✉)
Aerospace and Mechanical Engineering Department,
The University of Arizona, Tucson, AZ 85721, USA
e-mail: mr.moosavi@yahoo.com

models in 3D. Unless explicitly modeling crack faces as domain boundaries it is necessary in modeling fracture to include a means of introducing the displacement jump that occurs across the crack. In the XFEM this jump is introduced by extrinsically enriching the displacement approximation. In meshless methods, such as the EFGM, intrinsic approaches are most popular using either the visibility criterion or the diffraction method. The former is simpler to implement, especially for 3D problems, but leads to spurious crack extension (thus impairing accuracy) while the latter is accurate with no spurious extension problem but high computational complexity especially in 3D or with multiple cracks. So, the dilemma is that one would prefer to use the visibility criterion in 3D for economy but cannot guarantee accuracy due to spurious extension. On the other hand, an extrinsic enriched meshless method is developed for 3D fracture modeling where the crack tip is closed by modifying the nodal support and is similar to the idea used in the XFEM. However this method is not feasible when the crack front is curved in 3D. Alternatively the use of Lagrange multipliers is proposed and is later adopted in a number of subsequent papers which develop meshless methods for 3D fracture modeling. However this method involves additional unknowns which increase with the number of cracks. Besides which, the solution accuracy using this method, in terms of fracture parameters, is not clearly shown.

Crack propagation is an important failure mechanism in structural and mechanical systems. It requires accurate numerical models to implement essential simulation supporting failure prediction. The existence of system uncertainty and risk in loads, material properties, and crack size requires a reliability-based fracture-mechanics analysis to be taken into account. The objective of this work is to develop a new meshless methodology for predicting characteristics of structures containing crack-like defects.

This effort is based on a new integrated method entitled orthogonal meshless finite volume (OMFVM) (Moosavi et al. 2011a,b, 2008; Cheung et al. 1992; Daux et al. 2000) for determining crack-tip stress and strain fields. Such a coupling has the potential to greatly simplify crack-growth analysis while simultaneously achieving a substantially improved level of accuracy. The proposed research represents an advanced approach to computational modeling of crack by meshless methods. It will enable us in the development and improvement of this meshless method in crack problems and also it increases understanding of the fundamental issues of crack propagation in solid mechanics.

The OMFVM is based on local weak forms (LWFs) of governing equations and employs meshless interpolations for both the trial and the test functions. The trial functions are constructed by using the orthogonal moving least squares (OMLS) approximation. These approximations simply rely on the location of points or nodes in the body, rather than complex meshes. The key ingredients of the OMFVM may be summarized as: local weak formulation, OMLS interpolation, Petrov–Galerkin projection, evaluation of domain integrals appearing in the weak formulation, imposition of essential boundary conditions. The OMFVM has been successfully applied to several elastodynamic failure problems.

2 Governing equations

The governing differential equation for a linear elastic body undergoing infinitesimal deformations can be obtained by the linear momentum balance as

$$\mu(u_{i,jj} + u_{j,ij}) + \lambda u_{k,kj}\delta_{ij} + b_i = \rho\ddot{u}_i \tag{1}$$

with the boundary conditions

$$u_i = \bar{u}_i \qquad \text{on } \Gamma_u \tag{2a}$$

$$t_i = \sigma_{ij}n_j = \bar{t}_i = \mu(\bar{u}_{i,j} + \bar{u}_{j,i})n_j + \lambda\bar{u}_{k,k}n_j\delta_{ij} \quad \text{on } \Gamma_t \tag{2b}$$

$$\begin{aligned} t_i^c &= \sigma_{ij}^+ n_j^+ = \mu(u_{i,j}^+ + u_{j,i}^+)n_j^+ + \lambda u_{k,k}^+ n_j^+\delta_{ij} \\ &= \sigma_{ik}^- n_k^- = \mu(u_{i,k}^- + u_{k,i}^-)n_k^- + \lambda u_{l,l}^- n_k^-\delta_{ik} \quad \text{on } \Gamma_c \end{aligned} \tag{2c}$$

where the first two terms in Eq. (1) are equivalence to the stress tensor σ_{ij}, λ and μ are the Lame's coefficients and b_i is the body force. In Eq. (2), $\bar{u}_i$ is the prescribed displacements on the displacement boundary Γ_u, $\bar{t}_i$ and $\bar{u}_{i,j}$ are the prescribed tractions and displacement derivatives on the traction boundary Γ_t, respectively, n_j is the unit vector outward normal to the boundary Γ, and superscript and subscript c denote a crack.

Using the MLS approximation, the trial function in a local subdomain Ω_s is

$$u(\mathbf{x}) = \mathbf{p}^T(\mathbf{x})\mathbf{T}^T\mathbf{a}(\mathbf{x}) \qquad \forall \mathbf{x} \in \Omega_s \tag{3}$$

where $\mathbf{p}^T(\mathbf{x})$ is a monomial basis, $\mathbf{T}$ is a transformation lower triangular matrix which is defined as follows

$$\mathbf{T} = [t_{ij}] = \begin{cases} 0 & i < j \\ 1 & i = j \end{cases} \tag{4}$$

$\mathbf{a}(\mathbf{x})$ is a vector containing coefficients which are determined by minimizing a weighted discrete L_2 norm with respect to nodal points, defined as

$$J(\mathbf{x}) = \sum_{I=1}^{n} w_I(\mathbf{x})[\mathbf{p}^T(\mathbf{x_I})\mathbf{T}^T\mathbf{a}(\mathbf{x}) - \mathbf{u}(\mathbf{x}_I)]^2 = [\mathbf{TPa}(\mathbf{x}) - \mathbf{u}]^T\mathbf{W}[\mathbf{TPa}(\mathbf{x}) - \mathbf{u}] \quad (5)$$

where $w_I(\mathbf{x})$ is the weight function associated with the node I, with $w_I(\mathbf{x}) > 0$ for all $\mathbf{x}$ in the support of $w_I(\mathbf{x})$, $\mathbf{x_I}$ denote the value of $\mathbf{x}$ at node I, n is the number of nodes in Ω_s for which the weight functions $w_I(\mathbf{x}) > 0$. The stationarity of J in Eq. (5) with respect to $\mathbf{a}(\mathbf{x})$ leads to the following linear relation between $\mathbf{a}(\mathbf{x})$ and $\mathbf{u}(\mathbf{x}_I)$.

$$\mathbf{TA}(\mathbf{x})\mathbf{T}^T\mathbf{a}(\mathbf{x}) = \mathbf{TB}(\mathbf{x})\mathbf{u} \quad (6)$$

where the matrices $\mathbf{A}(\mathbf{x})$ and $\mathbf{B}(\mathbf{x})$ are defined by

$$\mathbf{A}(\mathbf{x}) = \mathbf{P}^T\mathbf{WP} = \sum_{i=1}^{n} w_i(x)\mathbf{p}(\mathbf{x}_i)\mathbf{p}^T(\mathbf{x}_i) \quad (7)$$

$$\mathbf{B}(\mathbf{x}) = \mathbf{P}^T\mathbf{W} = [w_1(\mathbf{x})p(\mathbf{x}_1), w_2(\mathbf{x})p(\mathbf{x}_2), \ldots, w_n(\mathbf{x})p(\mathbf{x}_n)] \quad \forall \mathbf{x} \in \Omega_s \quad (8)$$

The MLS approximation is well defined only when the matrix $\mathbf{A}$ in Eq. (6) is non-singular. The shape function may be found as

$$u(\mathbf{x}) = \mathbf{p}^T(\mathbf{x})\mathbf{T}^T(\mathbf{TA}(\mathbf{x})\mathbf{T}^T)^{-1}\mathbf{TB}(\mathbf{x})\mathbf{u} = \mathbf{\Phi}^T(\mathbf{x})\mathbf{u} \quad \forall \mathbf{x} \in \Omega_s \quad (9)$$

In this work, weight function is a fourth order spline as below

$$w_I(x) = \begin{cases} 1-6\left(\frac{d_I}{r_I}\right)^2+8\left(\frac{d_I}{r_I}\right)^3-3\left(\frac{d_I}{r_I}\right)^4 & 0 \le d_I \le r_I \\ 0 & d_I \ge r_I \end{cases} \quad (10)$$

where $d_I = |\mathbf{x} - \mathbf{x}_I|$ is the summation of Euclidean distance from node $\mathbf{x}_I$ to point $\mathbf{x}$; and r_I is the size of the support for the weight function w_I, which determines the support of node $\mathbf{x}_I$. The shape function $\mathbf{\Phi}(\mathbf{x})$, Eq. (9), can be calculated directly without any ill-conditioning or singularity which is the important benefit of the method.

A crack can be modeled as follows

$$u(\mathbf{x}) = \mathbf{\Phi}^T(\mathbf{x})\mathbf{u} + u^c(\mathbf{x}) = \mathbf{\Phi}^T(\mathbf{x})\mathbf{u} + \mathbf{\Phi}^T(\mathbf{x})\mathbf{H}(\mathbf{x})\boldsymbol{\alpha} + \mathbf{\Phi}^T(\mathbf{x})\mathbf{B}(\mathbf{x})\boldsymbol{\beta} \quad (11)$$

where u^c is crack displacement, $\mathbf{H}(\mathbf{x})$ the Heaviside step function, $\boldsymbol{\alpha}$ and $\boldsymbol{\beta}$ are additional unknowns, and $\mathbf{B}(\mathbf{x})$ is the Westergaard expansion as

$$\mathbf{B}(\mathbf{x}) = \left\{\sqrt{r}\sin\frac{\theta}{2}, \sqrt{r}\cos\frac{\theta}{2}, \sqrt{r}\sin\frac{\theta}{2}\sin\theta, \sqrt{r}\cos\frac{\theta}{2}\sin\theta\right\} \quad (12)$$

where r and θ are the local polar coordinate system at the crack tip. The first term on the right hand side is referring to a node in support of $\mathbf{x}$, the second term refers the set of nodes having its support completely cut by a crack, and the last term refers all the nodes each having a crack tip inside its support.

The finite volume (FV) discretization is based on the integral form of the equation over the control volume or sub-domain Ω_s. In other words, the FV discretization uses the integral form of Eq. (1) over the sub-domain Ω_s around node I as

$$\int_{\Omega_s}[\mu(u_{i,jj} + u_{j,ij}) + \lambda u_{k,kj}\delta_{ij} + b_i - \rho\ddot{u}_i]d\Omega = 0 \quad (13)$$

Applying the divergence theorem to the first integral term gives

$$\int_{\partial\Omega_s}[\mu(u_{i,j} + u_{j,i})n_j + \lambda u_{k,k}n_j\delta_{ij}]d\Gamma + \int_{\Omega_s} b_i d\Omega + \int_{\Omega_s}\rho\ddot{u}_i d\Omega = 0 \quad (14)$$

where n_j is the outward normal to the local boundary $\partial\Omega_s$. At this point, the conservative nature of the FVM is established as the flux, stress σ_{ij}, is integrated over the local boundary $\partial\Omega_s$.

By considering the traction boundary conditions from Eq. (2) and imposing it in Eq. (14) leads to

$$\int_{L_s}[\mu(u_{i,j} + u_{j,i})n_j + \lambda u_{k,k}n_j\delta_{ij}]d\Gamma + \int_{\Gamma_{su}}[\mu(u_{i,j} + u_{j,i})n_j + \lambda u_{k,k}n_j\delta_{ij}]d\Gamma + \int_{\Gamma_{st}}[\mu(u_{i,j} + u_{j,i})n_j + \lambda u_{k,k}n_j\delta_{ij}]d\Gamma + \int_{\Omega_s} b_i d\Omega + \int_{\Omega_s}\rho\ddot{u}_i d\Omega = 0 \quad (15)$$

The Eq. (15) represents a physical meaning in the balance law of the local sub-domain Ω_s as conventional FVM with the traction boundary conditions being enforced. Hence it is called orthogonal meshless finite volume (OMFV) formulation of the equilibrium equation. The displacement can be interpolated with the shape function as in Eq. (11)

$$u_i(\mathbf{x}) = \sum_{J=1}^{n} \Phi^{(J)}(\mathbf{x}) u_i^{(J)} + \sum_{K=1}^{n_c} \Phi^{(K)}(\mathbf{x}) \mathrm{H}^{(K)}(\mathbf{x}) \alpha_i^{(K)} + \sum_{L=1}^{n_t} \Phi^{(L)}(\mathbf{x}) \mathrm{B}^{(L)}(\mathbf{x}) \beta_i^{(L)} \tag{16}$$

where n_c is the set of nodes having its support completely cut by a crack, and n_t is the set of nodes each having a crack tip inside its support.

At now, Eq. (15) is discretized by substituting Eq. (16)

$$\begin{aligned}
&\sum_{J=1}^{n} \left[\int_{\Omega_s} \rho \Phi^{(J)} d\Omega \right] \ddot{u}_i^{(J)} + \sum_{K=1}^{n_c} \left[\int_{\Omega_s} \rho \Phi^{(K)} \mathrm{H}^{(K)} d\Omega \right] \ddot{\alpha}_i^{(K)} \\
&\quad + \sum_{L=1}^{n_t} \left[\int_{\Omega_s} \rho \Phi^{(L)} \mathrm{B}^{(L)} d\Omega \right] \ddot{\beta}_i^{(L)} \\
&\quad - \sum_{J=1}^{n} \left[\int_{L_s} \mu \Phi_{,j}^{(J)}(x) n_j d\Gamma + \int_{\Gamma_{su}} \mu \Phi_{,j}^{(J)}(x) n_j d\Gamma \right] u_i^{(J)} \\
&\quad - \sum_{K=1}^{n_c} \left[\int_{L_{sc}} \mu \Phi_{,j}^{(K)}(x) \mathrm{H}^{(K)} n_j d\Gamma + \int_{\Gamma_{suc}} \mu \Phi_{,j}^{(K)}(x) \mathrm{H}^{(K)} n_j d\Gamma \right] \alpha_i^{(K)} \\
&\quad - \sum_{L=1}^{n_t} \left[\int_{L_{sc}} \mu \Phi_{,j}^{(L)}(x) \mathrm{B}^{(L)} n_j d\Gamma + \int_{\Gamma_{suc}} \mu \Phi_{,j}^{(L)}(x) \mathrm{B}^{(L)} n_j d\Gamma \right] \beta_i^{(L)} \\
&\quad - \sum_{J=1}^{n} \left[\int_{L_s} \lambda \Phi_{,k}^{(J)}(x) n_j \delta_{ij} d\Gamma + \int_{\Gamma_{su}} \lambda \Phi_{,k}^{(J)}(x) n_j \delta_{ij} d\Gamma \right] u_k^{(J)} \\
&\quad - \sum_{K=1}^{n_c} \left[\int_{L_{sc}} \lambda \Phi_{,k}^{(K)}(x) \mathrm{H}^{(K)} n_j \delta_{ij} d\Gamma + \int_{\Gamma_{suc}} \lambda \Phi_{,k}^{(K)}(x) \mathrm{H}^{(K)} n_j \delta_{ij} d\Gamma \right] \alpha_k^{(K)} \\
&\quad - \sum_{L=1}^{n_t} \left[\int_{L_{sc}} \lambda \Phi_{,k}^{(L)}(x) \mathrm{B}^{(L)} n_j \delta_{ij} d\Gamma + \int_{\Gamma_{suc}} \lambda \Phi_{,k}^{(L)}(x) \mathrm{B}^{(L)} n_j \delta_{ij} d\Gamma \right] \beta_k^{(L)} \\
&= \int_{\Gamma_{st}} [\mu (\bar{u}_{i,j} + \bar{u}_{j,i}) n_j + \lambda \bar{u}_{k,k} n_j \delta_{ij}] d\Gamma \\
&\quad + \int_{\Gamma_{stc}} \left[\mu (u_{i,j}^{+} + u_{j,i}^{+}) n_j^{+} + \lambda u_{k,k}^{+} n_j^{+} \delta_{ij} \right] d\Gamma + \int_{\Omega_s} b_i d\Omega
\end{aligned} \tag{17}$$

The relation between displacement and force is obtained as

$$\mathbf{M}\ddot{\mathbf{u}} + \mathbf{K}\mathbf{u} = \mathbf{f} \tag{18}$$

where

$$\begin{aligned}
M_{ij} = &\sum_{J=1}^{n} \left[\int_{\Omega_s} \rho \Phi^{(J)} d\Omega \right] \ddot{u}_i^{(J)} \\
&+ \sum_{K=1}^{n_c} \left[\int_{\Omega_s} \rho \Phi^{(K)} \mathrm{H}^{(K)} d\Omega \right] \ddot{\alpha}_i^{(K)} \\
&+ \sum_{L=1}^{n_t} \left[\int_{\Omega_s} \rho \Phi^{(L)} \mathrm{B}^{(L)} d\Omega \right] \ddot{\beta}_i^{(L)}
\end{aligned} \tag{19}$$

is the mass matrix, $\ddot{\mathbf{u}}$ the acceleration vector,

$$\begin{aligned}
K_{ij} = &- \sum_{J=1}^{n} \left[\int_{L_s} \mu \Phi_{,j}^{(J)}(x) n_j d\Gamma + \int_{\Gamma_{su}} \mu \Phi_{,j}^{(J)}(x) n_j d\Gamma \right] u_i^{(J)} \\
&- \sum_{K=1}^{n_c} \left[\int_{L_{sc}} \mu \Phi_{,j}^{(K)}(x) \mathrm{H}^{(K)} n_j d\Gamma + \int_{\Gamma_{suc}} \mu \Phi_{,j}^{(K)}(x) \mathrm{H}^{(K)} n_j d\Gamma \right] \alpha_i^{(K)} \\
&- \sum_{L=1}^{n_t} \left[\int_{L_{sc}} \mu \Phi_{,j}^{(L)}(x) \mathrm{B}^{(L)} n_j d\Gamma + \int_{\Gamma_{suc}} \mu \Phi_{,j}^{(L)}(x) \mathrm{B}^{(L)} n_j d\Gamma \right] \beta_i^{(L)} \\
&- \sum_{J=1}^{n} \left[\int_{L_s} \lambda \Phi_{,k}^{(J)}(x) n_j \delta_{ij} d\Gamma + \int_{\Gamma_{su}} \lambda \Phi_{,k}^{(J)}(x) n_j \delta_{ij} d\Gamma \right] u_k^{(J)} \\
&- \sum_{K=1}^{n_c} \left[\int_{L_{sc}} \lambda \Phi_{,k}^{(K)}(x) \mathrm{H}^{(K)} n_j \delta_{ij} d\Gamma + \int_{\Gamma_{suc}} \lambda \Phi_{,k}^{(K)}(x) \mathrm{H}^{(K)} n_j \delta_{ij} d\Gamma \right] \alpha_k^{(K)} \\
&- \sum_{L=1}^{n_t} \left[\int_{L_{sc}} \lambda \Phi_{,k}^{(L)}(x) \mathrm{B}^{(L)} n_j \delta_{ij} d\Gamma + \int_{\Gamma_{suc}} \lambda \Phi_{,k}^{(L)}(x) \mathrm{B}^{(L)} n_j \delta_{ij} d\Gamma \right] \beta_k^{(L)}
\end{aligned} \tag{20}$$

is the stiffness matrix, $\mathbf{u}$ is the displacement vector, and

$$\begin{aligned}
f_i = &\int_{\Gamma_{st}} [\mu (\bar{u}_{i,j} + \bar{u}_{j,i}) n_j + \lambda \bar{u}_{k,k} n_j \delta_{ij}] d\Gamma \\
&+ \int_{\Gamma_{stc}} \left[\mu \left(u_{i,j}^{+} + u_{j,i}^{+} \right) n_j^{+} + \lambda u_{k,k}^{+} n_j^{+} \delta_{ij} \right] d\Gamma \\
&+ \int_{\Omega_s} b_i d\Omega
\end{aligned} \tag{21}$$

is the force vector.

3 Numerical examples

This method is evaluated by the following examples. Those are presented to illustrate the implementation, accuracy and efficiency of the present OMFVM approach.

Example 1 Plate with a middle crack subjected to traction

This first example presents a middle cracked plate, fixed at the bottom and subjected to a traction load $P = 1$ applied on the right, as shown in Fig. 1. The dimensions of the plate are length $l = 0.052$ m and width $h = 0.08$ m. The a/h ratio is 0.2. The elastic modulus and Poisson's ratio are 75.6 GPa and 0.286, respectively, and $\rho = 2{,}450\,\mathrm{kg/m^3}$.

We consider two cases in this problem; in the first one, the crack remains stationary during simulation and in the second case, the crack remains stationary until 4.4 μs and then propagates with a constant velocity $v = 1{,}000$ m/s along its original direction. The stress intensity histories computed for both cases and are shown in Fig. 2.

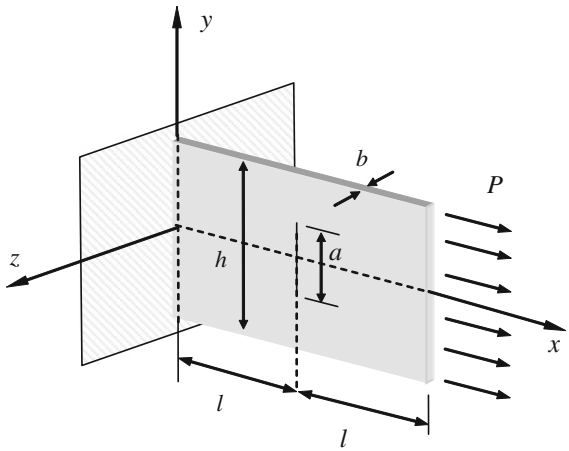

Fig. 1 A plate with middle crack under a traction load

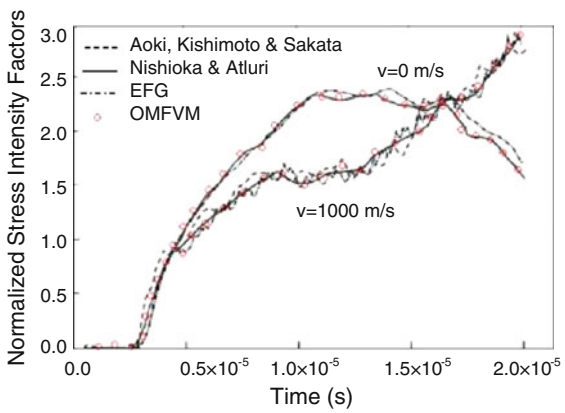

Fig. 2 Time-dependence of the mode I dynamic stress intensity factors for the plate with a middle crack

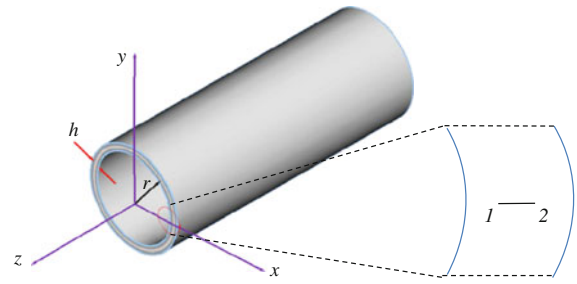

Fig. 3 A cylinder with a crack subjected to impact internal pressure

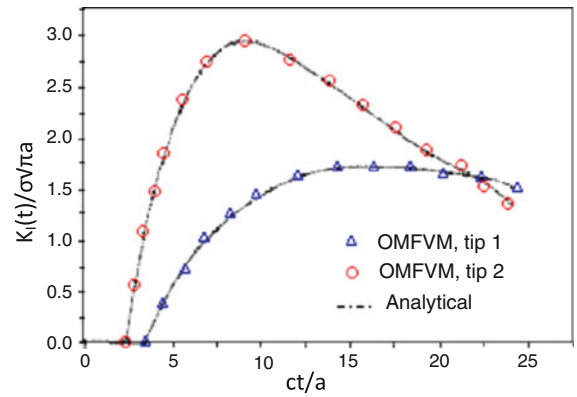

Fig. 4 Normalized dynamic stress intensity factors versus normalized time

As indicated in Fig. 2, there is a good agreement between the results of the OMFVM and the ones of previous methods like as element free Galerkin (EFG) method, Aoki et al. (1987), Nishioka and Atluri (1980), Belytschko et al. (1995).

Example 2 Cylinder with a crack subjected to impact internal pressure

We examine the case of a cylinder with a crack subjected to impact internal pressure, as shown in Fig. 3. We assume elastic modulus $E = 8 \times 10^{10}$ Pa, Poisson's ratio $\nu = 0.29$, and $\rho = 7{,}800\,\mathrm{Kg/m^3}$. An impact internal pressure of P is applied. The stress intensity factors (SIF) K_I at tips of crack are computed and compared in Fig. 4 with the analytical solution. In this figure, $c = \sqrt{E/\rho}$ and a is the length of crack. As indicated in this figure, there is a good agreement between of the results of OMFVM and the analytical ones, Zahoor (1991).

Example 3 Plate with a central crack under shear

In third example, a plate with a central crack is considered, as indicated in Fig. 5. The geometrical dimen-

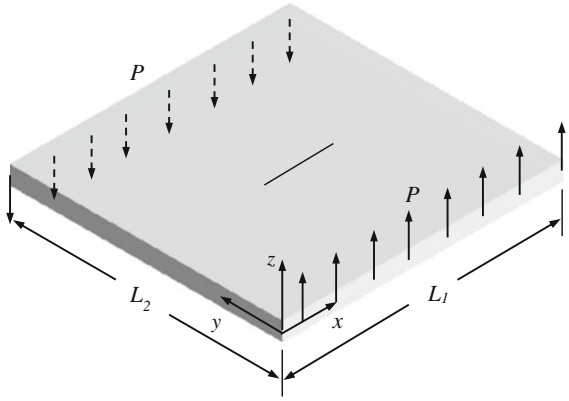

Fig. 5 A plate with a central crack under shear

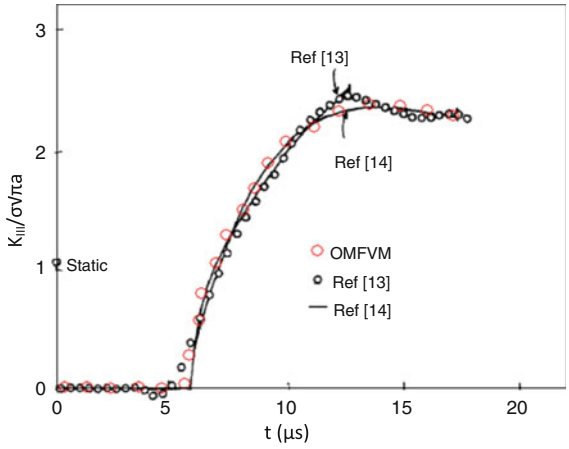

Fig. 6 Time variation of normalized dynamic stress intensity factor mode III for stationary crack

sions of the plate are $L_1 = 104$ and $L_2 = 40$ mm. The material properties are $\rho = 2.45 \times 10^3$ kg/m^3 and $E = 2.94 \times 10^{10}$ Pa. The applied shear load is $P = 9.8 \times 10^6$ Pa. The normalized dynamic stress intensity factor $K_{III}/\sigma\sqrt{\pi a}$ for mode III deformation for a stationary crack of the length $a = 12$ mm are shown in Fig. 6.

The analytical results for a crack in an infinite plate by Kostrov (1966) and Ravera and Sih (1970) are also illustrated in Fig. 6. The present result agrees well with the analytical ones. Figure 7 demonstrate the time variation of $K_{III}(t)/\sigma\sqrt{\pi a}$ of the crack with the initial length $a = 16$ mm which propagates from $t = 7\,\mu$s with the constant velocity $c = 1,000$ m/s. The result agrees well with the analytical one by Achenbach (1970).

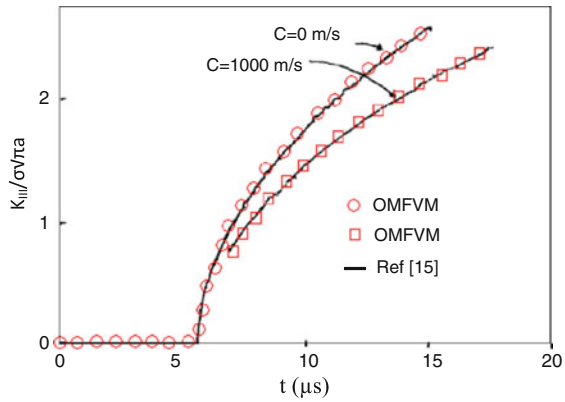

Fig. 7 Time variation of normalized dynamic stress intensity factor mode III for propagating crack

4 Conclusion

This paper presented the OMFVM applied to elastodynamic crack problems. The OMFVM unifies the major advantages of meshless methods and finite volume method in one single scheme. In the LWF of the governing differential equation, an OMLS interpolation was used to form the approximations to the solution known as trial functions. A new displacement function is used at the tip of the crack to give a new OMFVM. Because of applying the orthogonal moving least square approximation instead of the moving least square, this method does not have any singularity or ill-conditioning in calculation of the shape function. Also the method has a great computational precision. The OMFVM method was applied to and passed several test crack problems. Very good results from the method was obtained.

References

Achenbach JD (1970) Extension of a crack by a shear wave. ZAMP 21:887–900

Aoki S, Kishimoto K, Sakata M (1987) Finite element computation of dynamic stress intensity factor for a rapidly propagating crack using 3-integral. Comput Mech 62(2):54–62

Belytschko T, Lu YY, Gu L (1994) Element-free Galerkin methods. Int J Numer Methods Eng 37:229–256

Belytschko T, Lu YY, Gu L, Tabbara M (1995) Element-free Galerkin methods for static and dynamic fracture. Int J Solids Struct 32:2547–2570

Cheung Y, Wang Y, Woo C (1992) A general method for multiple crack problems in a finite plate. Comput Mech 10:335–343

Daux C, Moes N, Dolbow J, Sukumar N, Belytschko T (2000) Arbitrary branched and intersecting cracks with

the extended finite element method. Int J Numer Methods Eng 48:1741–1760
Kostrov BV (1966) Unsteady propagation of longitudinal shear cracks. J Appl Math Mech 30:1241–1248
Monaghan JJ (1982) Why particle methods work. SIAM J Sci Stat Comput 3:422–433
Monaghan JJ (1988) An introduction to SPH. Comput Phys Commun 48:89–96
Moosavi MR, Khelil A (2008) Accuracy and computational efficiency of the finite volume method combined with the meshless local Petrov–Galerkin in comparison with the finite element method in elasto-static problem. ICCES 5(4):211–238
Moosavi MR, Delfanian F, Khelil A (2011a) Orthogonal meshless finite volume method in elasticity. Thin Walled Struct 49(6):708–712
Moosavi MR, Delfanian F, Khelil A (2011b) The orthogonal meshless finite volume method for solving Euler-Bernoulli beam and thin plate problems. Thin Walled Struct 49(7):923–932
Nishioka T, Atluri SN (1980) Numerical modeling of dynamic crack propagation in finite bodies, by moving singular elements. Part 2: results. J Appl Mech 47:577–582
Ravera RJ, Sih GC (1970) Transient analysis of stress waves around cracks under antiplane strain. J Acoust Soc Am 47:875–881
Zahoor A (1991) Ductile fracture handbook. Novetech Corp., Rockville